Performance characterization methods for absorption chillers applied to an NH3-LiNO3 single-stage prototype

Amín Altamirano, Nolwenn Le Pierrès, Benoit Stutz, Alberto Coronas

Version of Record: https://www.sciencedirect.com/science/article/pii/S1359431120339132
Manuscript_769e8b7a840373585a6ef88e3d7382c1

Performance characterization methods for absorption chillers applied to an NH_3-$LiNO_3$ single-stage prototype

Amín Altamirano[1,2], Nolwenn Le Pierrès[1], Benoit Stutz[1,*], Alberto Coronas[2]

[1] *LOCIE Laboratory, Université Savoie Mont Blanc, CNRS UMR5271, Savoie Technolac, 73376 Le Bourget Du Lac (France)*

[2] *CREVER—Group of Applied Thermal Engineering, Mechanical Engineering Dept., Universitat Rovira i Virgili, Av. Països Catalans 26, 43007 Tarragona (Spain)*

Abstract

Absorption chillers require precise models for their control and optimization. The present work analyzes the behavior of a 10-kW absorption chiller by means of four different methods that use the external fluid temperatures to situate the machine operating conditions, either through a characteristic temperature difference or through the COP_{carnot}. The studied models are of different physical insight levels: a semi-empirical method (the characteristic equation method), two empirical methods (the adapted characteristic equation method and the Carnot function model), and a thermodynamic model, here called the "effectiveness model," based on thermal and mass effectivenesses. The COP_{carnot} is used for the first time as a common parameter to situate the results from the different models and the effectivenessses of the components. Different from previous models presented in the literature, the proposed effectiveness model is able to account for the non-equilibrium conditions of the solution with the vapor phase at the inlet and outlet of the sorption exchangers. Therefore, owing to a better understanding of the internal machine behavior, it allowed for the identification of thermal and electric COP improvement opportunities.

Highlights

- The characterization of an NH_3-$LiNO_3$ absorption chiller.
- The use of the characteristic equation method.
- The use of empirical models to characterize an absorption chiller.
- Thermodynamic model based on thermal and mass effectivenesses.

Keywords

Absorption chiller, ammonia, lithium nitrate, characteristic equation, thermal effectiveness, mass effectiveness

[*]= corresponding author details, E-mail: benoit.stutz@univ-smb.fr, Phone Number: +33 (0)4 79 75 88 14, Fax Number: +33 (0) 4 79 75 81 44

Nomenclature		**Subscripts and superscripts**	
A	enthalpy coefficient (-)	*0*	Carnot function model y-intercept
a	characteristic parameter (-)	*a*	absorber
B	isostere slope in a Dühring chart (-)	*abs*	absorption
b	characteristic parameter (-)	*ac*	absorber/condenser parallel flow
C	enthalpy coefficient (-)	*ad*	adiabatic
c	characteristic parameter (-)	*avg*	average
CE	characteristic equation	*c*	condenser or characteristic equation variable
CFM	Carnot function model	*c'*	adapted characteristic equation variable
COP	coefficient of performance (-)	*cfm*	Carnot function model
e	characteristic parameter (-)	*corr*	correlated
EM	effectiveness model	*e*	evaporator
F	Carnot function model parameter (-)	*eq*	equilibrium
G	enthalpy coefficient (-)	*exp*	experimental
h	specific enthalpy (kJ kg^{-1})	*g*	generator
M	mass content (kg)	*htf*	heat transfer fluid
$\dot{m}$	mass flow rate (kg s^{-1})	*h*	high
P	pressure (kPa)	*i*	inlet
$\dot{Q}$	heat transfer rate (kW)	*iso*	isothermal
R	equilibrium factor (-)	*l*	low
Re	Reynolds number (-)	*loss*	solution heat exchanger loss
r	characteristic parameter (-)	*m*	mass
s	characteristic parameter (kW K^{-1})	*max*	maximum
s'	characteristic parameter (-)	*nom*	nominal
T	internal temperature (°C)	*o*	outlet
t	external temperature (°C)	*p*	pump
UA	heat transmission (kW K^{-1})	*sat*	saturation
$\dot{V}$	volumetric flow rate (m^3 h^{-1})	*sol*	solution
x	concentration (% w.t.)	*sorp*	sorption
z	arithmetic temperature difference correction factor	*st*	storage tank
		th	thermal
		v	vapor
Greek letters			
α	characteristic parameter (-)		
Δ	differential quantity		
$\Delta\Delta t$	characteristic temperature difference (K)		
$\Delta\Delta t'$	adapted characteristic temperature difference (K)		
$\Delta\Delta t_{min}$	minimum temperature difference (K)		
ε	effectiveness		
μ	dynamic viscosity (Pa s)		
ν	kinematic viscosity (mm^2 s^{-1})		
τ	Carnot function model parameter (-)		
ω	Carnot function model parameter (-)		

1. Introduction

Cooling generation is and will continue to be an important issue in the future. In the building sector alone, the need for space cooling has more than tripled in 16 years (from 1990 to 2016) and will triple again by 2050 [1]. This increase in cooling demand has created important challenges for the environment and the electricity distribution grid in hot-climate countries like Spain [2], and in some regions of the world represents over 70% of peak residential electrical demand during hot days [1].

Absorption chillers represent an alternative to the conventional vapor compression systems as they can run on renewable energy sources and waste heat [3]. These systems, which replace the mechanical compression of conventional systems by a thermochemical compression, are more suitable for conditions in which heat is largely available at low prices [4]. Moreover, their implementation could contribute to the balance of energy flows and help reduce the load on the electricity supply system [5].

Absorption chillers are more complex machines than vapor compression systems. Their modeling is of fundamental importance for the evaluation and characterization of their performance, especially when they are operated outside their nominal conditions. The different existing models can be divided into three categories depending on their nature: white box (physical), when it contains complete insight into the physical process or system; gray box (semi-empirical), when there is some degree of physical insight and the model parameters can be physically interpreted; and black box (empirical), when no physical insight is necessary and the model describes a dataset of experimental results [6,7]. The characteristic equation (CE) method is a gray-box-type model commonly used for modeling of absorption chillers as it allows the thermal loads of the components to be calculated by means of simple linear functions [7]. In this method as in most of the methods (physical or semi-empirical) present in the literature, the sorption phenomena (i.e., the absorption and desorption) are considered to be controlled by the heat transfer and the solution is considered to reach equilibrium conditions with the vapor phase at the outlet (i.e., the solution has used its entire absorption/desorption potential at a point at which, at the outlet, the temperature, pressure, and chemical local potential between the phases is equal and, therefore, there are no more transfers between them [8]) of the components (i.e., the absorber and generator), which is never the case in real operating conditions [9]. Moreover, the overall heat transfer coefficient employed to regroup both the heat and mass transfer phenomena is considered constant during the entire range of operating conditions. Owing to these and other simplifying assumptions, the characteristic equation method possesses considerable deviations from the experimental results. An alternative to this is the use of empirical methods based on numerical fits of the experimental results. In this regard, Kühn and Ziegler [10] and Boudéhenn et al. [11] presented the "adapted characteristic equation (CE) method" and the "Carnot function model (CFM)," respectively. The former is based on the characteristic equation method and uses an arbitrary parameter to estimate the evaporator/generator heat rates as linear functions, whereas the latter represents the cooling capacity and the thermal COP as functions of the chiller COP_{carnot}. Despite the increase in the accuracy of these models compared with the CE method, the underlying physical mechanisms of the machine operation are hidden at all times [12].

In sorption exchangers, even though heat and mass transfers are coupled, they are separate processes and either of them can control the overall transfer process [8]. Therefore, a more precise approach can be the implementation of an effectiveness model (EM) that considers both the heat and mass transfer as independent. In this regard, a physical (thermodynamic) model of a small-capacity NH_3-$LiNO_3$ pre-industrial prototype [13] has been developed based on thermal and mass effectivenesses that takes into account the non-equilibrium conditions of the solution with the vapor phase in the machine (i.e., conditions at which, at a given vapor pressure and solution concentration, the solution is at a subcooled ($T_{sol} < T_{sol}^{eq}$) or super-heated ($T_{sol} > T_{sol}^{eq}$) state), which facilitates a better consideration of the sensible heat effects on the sorption elements. To the best of our knowledge, no physical model has been presented before with similar characteristics for the characterization of absorption chillers. The present work shows the characterization of the prototype by the CE method, the adapted CE

method, the CFM, and the EM. All the studied models use the external heat transfer fluid temperatures to situate the machine operating conditions, either through a characteristic temperature difference (in the case of the CE-based models) or through the COP_{carnot}. The use of the external temperatures in the modelling of absorption chillers results very practical since these are variables that are easily obtained during the machine operation with barely no need of additional instrumentation. Furthermore, the manufacturers use these variables for the characterization of commercial chillers. The results from the CE-based models and the effectivenesses of the exchangers are for the first time represented in the COP_{carnot} domain, giving a different perspective on their interpretation. Additionally, models with different insight levels were selected to discuss on their advantages and disadvantages depending on the user requirements. The thermodynamic model, being the one with the most complete physical insight into the machine, was used to analyze the individual exchanger performances and the internal thermodynamic non-equilibrium conditions of the solution with the vapor phase under part-load conditions. A better understanding of the machine allowed us to identify opportunities for thermal and electric COP improvements.

2. System description

The machine is a 10-kW water-cooled NH_3-$LiNO_3$ single-stage absorption chiller fully equipped with brazed plate heat exchangers (BPHE) in all its thermal components [13], inspired by a previously published patent [14]. A simplified diagram of the machine is shown in Figure 1. In this system, the diluted solution coming from the solution storage tank is pre-heated in the SHX, after which it enters the generator to absorb heat and desorb NH_3 vapor. The desorbed vapor is then condensed and the liquid refrigerant is stored in a refrigerant storage tank. Depending on the cooling requirements and low operating pressure (P_l), the refrigerant expansion valve (REV) allows for the flow of refrigerant through the evaporator, after which the vapor is sent to the plate absorber where the concentrated solution (coming from the generator and pre-cooled in the solution heat exchanger [SHX]) absorbs it while it is cooled down by an external fluid. The resulting solution is then sent to the solution storage tank, where the process starts again.

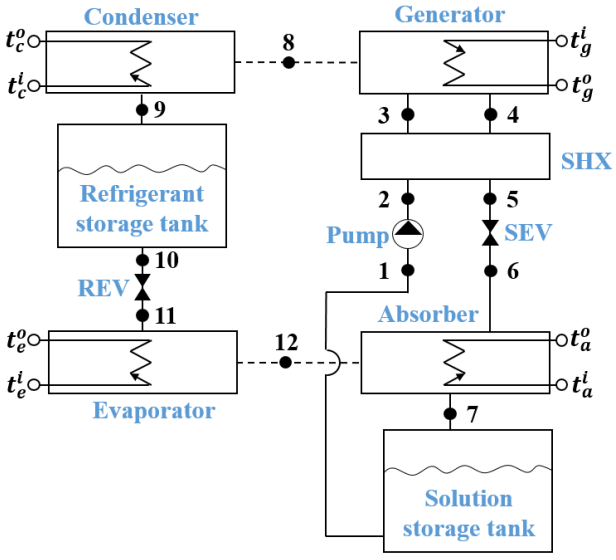

Figure 1. Simplified diagram of the 10-kW NH_3-$LiNO_3$ water-cooled absorption chiller developed by Zamora [13].

During experiments, the heat transfer fluid (HTF; water) of the heat sink flowed in parallel through the condenser and the absorber ($t_c^i = t_a^i = t_{ac}^i$). The nominal operating conditions of the chiller were defined at an inlet generator temperature (t_g^i) of 90 °C, an intermediate cooling temperature (t_{ac}^i) of 37.5 °C, and a chilled water temperature (t_e^o) of 15°C [13]. The machine was characterized under part-load operation with the conditions and accuracies shown in Table 1. The cooling and generator heat

rates were directly calculated using temperature measurements (inlet/outlet) from PT-100 probes and flow rate measurements from magnetic flowmeters. Regarding the heat sink, temperature measurements were performed at the inlet and outlet of the parallel source, and the HTF flow rate and exchanged heat were indirectly calculated using a global energy balance assuming no heat losses with the environment. Finally, considering the technical data of the solution pump and the pressure losses in the circuit, the solution mass flow rate was calculated to be approximately 0.12 kg s^{-1} (with an uncertainty of $\pm 4\%$). The experimental results of the characterization test campaign, obtained from [13], are presented in Table 2.

Table 1. Operating conditions of the characterized NH_3-$LiNO_3$ absorption chiller prototype [13].

Variable	Measurement values or ranges	Uncertainty
$t_e^o\ (°C)$	8.4; 15.5	±0.1 °C
$t_{ac}^i\ (°C)$	30–40.2	±0.1 °C
$t_g^i\ (°C)$	85; 90; 95	±0.1 °C
$\dot{v}_e\ (m^{-3}\ h^{-1})$	3	±0.5 %
$\dot{v}_{ac}\ (m^{-3}\ h^{-1})$	6	±4.7 %
$\dot{v}_g\ (m^{-3}\ h^{-1})$	3	±0.5 %
$\dot{Q}_e\ (kW)$	3.15–17.82	±0.5 kW
$\dot{Q}_{ac}\ (kW)$	11.62–46.08	±0.71 kW
$\dot{Q}_g\ (kW)$	8.47–28.26	±0.5 kW
COP_{th}	0.37–0.65	±0.03

Table 2. Experimental results of the characterization test campaign of the NH_3- $LiNO_3$ absorption chiller prototype [13].

Test	t_{ac}^i $(°C)$	t_{ac}^o $(°C)$	t_e^i $(°C)$	t_e^o $(°C)$	t_g^i $(°C)$	t_g^o $(°C)$	$\dot{V}_{ac}$ $(m^{-3}\ h^{-1})$	$\dot{V}_e$ $(m^{-3}\ h^{-1})$	$\dot{V}_g$ $(m^{-3}\ h^{-1})$	$\dot{Q}_e$ (kW)	$\dot{Q}_g$ (kW)	COP
1	30	34.4	11.7	8.4	85	79.5	5.91	3.02	3	11.53	18.96	0.61
2	32	35.7	11.1	8.4	85	80.2	59.5	3	3	9.53	16.34	0.58
3	34	37	10.5	8.4	85	81	5.97	3.03	2.99	7.34	13.55	0.54
4	36	38.3	9.9	8.4	85	81.8	6.05	3.04	3.01	5.29	11.1	0.48
5	38	39.6	9.3	8.4	85	82.5	6.21	3.03	3.03	3.15	8.47	0.37
6	30	35	12	8.4	90	83.8	5.86	3	3	12.77	21.1	0.61
7	32	36.2	11.4	8.4	90	84.7	5.89	3.01	3	10.44	18.05	0.58
8	34	37.6	10.9	8.4	90	85.3	5.96	3.02	2.99	8.88	16.01	0.55
9	30	35.8	12.8	8.4	95	87.6	5.92	3	2.98	15.18	25.02	0.61
10	32	37	12.1	8.4	95	88.5	5.97	3.01	3	12.9	22.03	0.59
11	34	38.8	11.6	8.4	95	89.2	5.55	3.01	3	11.36	19.63	0.58
12	36	39.9	11	8.4	95.1	90.2	5.68	3.02	3	8.99	16.52	0.54
13	38	40.7	10.1	8.4	95	91.2	5.83	3.02	2.98	5.68	12.77	0.44
14	40	42.5	9.7	8.3	94.9	91.6	5.58	3.01	3	4.83	11.4	0.42
15	29.8	36	20.3	15.4	90	82.2	6.09	3.01	3	17.33	26.52	0.65
16	32.3	37.6	19.7	15.4	89.9	82.8	6.48	3.03	3.04	15.35	24.44	0.63
17	33.9	39.8	19.5	15.4	90	83.2	5.43	3.01	3	14.35	22.72	0.63
18	38.1	41.7	18.2	15.5	90	85.2	6.22	3.02	3.01	9.32	16.44	0.57
19	40.2	43	17.6	15.4	89.9	85.7	6.70	3.04	3	7.67	14.29	0.54
20	32	-	19.9	14.8	94.9	86.6	6.26	3.03	3.04	17.82	28.26	0.63
21	33.9	39.8	20.1	15.4	94.9	87.3	6.25	3.03	3	16.54	26.09	0.63
22	36	-	19.4	15.4	95	88.2	6.25	3.04	2.98	13.99	23.01	0.61
23	38.2	42.6	18.8	15.3	95	89	6.26	3.02	3.01	12.04	20.27	0.59
24	40.1	43.3	17.9	15.4	95	90.3	6.69	3.02	3.01	8.57	16.24	0.53

3. Characterization of the system

In this section, the different approaches to characterize the system within its range of operating conditions are presented. First, the original CE method is introduced, after which the adapted CE method and the CFM are presented. Finally, the EM based on thermal and mass effectivenesses is described. The CE-based methods use characteristic temperature differences ($\Delta\Delta t$ or $\Delta\Delta t'$) function of the external temperatures to represent the different operating conditions of the absorption chiller. However, these are not universal parameters as they are a result of the specific configuration of the machine studied (e.g., the machine capacity, the heat transfer coefficients, the working fluid properties, or the dataset used for the regression). In the present work, the Carnot coefficient of performance (COP_{carnot}) of the chiller was used as a common tool to situate the results of models of different nature over the entire range of operating conditions of the absorption chiller. The COP_{carnot} (Eq. (1)) represents the maximum theoretical efficiency of the chiller as a reversible process with isothermal heat transfers at the three temperature levels [15], allowing for the graphical comparison of different absorption chillers (regardless of their cooling capacity) [16] and modeling methods, as in the present study.

$$COP_{carnot} = \left(\frac{t_g^i - t_a^i}{t_g^i}\right)\left(\frac{t_e^o}{t_c^i - t_e^o}\right) \tag{1}$$

3.1. Characteristic equation method

The CE method is a semi-empirical method that was originally developed for single-stage H_2O-LiBr absorption chillers [17,18]. It has shown high flexibility as it has been adapted to other working pairs [19,20], direct-fired machines [21], and systems with adiabatic absorbers [22]. The most widespread method was presented by Hellmann et al. [18]. Its main goal is to represent the cooling capacity and thermal COP of the chiller as functions of the temperatures of the external HTFs. For this, the heat transfers in the main four components are represented as functions of the arithmetic mean temperatures of the internal (T) and external (t) fluids (Eqs. (2)-(5)). In these equations, z is the correction factor (due to the fact that logarithmic mean temperature differences are not taken into account).

$$\dot{Q}_e = UA_e \cdot z_e \cdot \left(t_e^{avg} - T_e^{sat}\right) \tag{2}$$

$$\dot{Q}_c = UA_c \cdot z_c \cdot \left(t_c^{avg} - T_c^{sat}\right) \tag{3}$$

$$\dot{Q}_a = UA_a \cdot z_a \cdot \left(t_a^{avg} - T_a^{avg}\right) \tag{4}$$

$$\dot{Q}_g = UA_g \cdot z_g \cdot \left(t_g^{avg} - T_g^{avg}\right) \tag{5}$$

Moreover, in the case of single-stage absorption chillers, the internal temperatures of the exchangers can be integrated into a single equation thanks to Dühring's rule expressing the saturation properties of the working fluid (Eq. (6)).

$$T_g^{avg} - T_a^{avg} = B \cdot (T_c^{sat} - T_e^{sat}) \tag{6}$$

On the basis of certain procedures described in [18], it is demonstrated that the evaporator and generator heat transfers can be expressed as functions of a total temperature difference $\Delta\Delta t$, defined by Eq. (7), which represents the difference between the "temperature thrust" ($t_g^{avg} - t_a^{avg}$) and the "temperature lift" ($t_c^{avg} - t_e^{avg}$) corrected with the Dühring coefficient (B). If a parallel flow is being used for the absorber and the condenser, their average external temperatures (t_a^{avg} and t_c^{avg}) can be replaced with the average external intermediate temperature (t_{ac}^{avg}).

$$\Delta\Delta t = t_g^{avg} - t_a^{avg} - B \cdot \left(t_c^{avg} - t_e^{avg}\right) \tag{7}$$

The thermal loads at the evaporator/generator and the COP are described by Eqs. (8)–(13), where A, C, and G are ratios of enthalpy differences of the internal components and $\dot{Q}_{loss}$ represents the SHX loss or, as defined by Hellmann et al. [18], the heat required in the generator for heating and rejected in the absorber for cooling the solution streams to the appropriate internal equilibrium temperatures. Finally, $\Delta\Delta t_{min}$ expresses the minimum total temperature difference ($\Delta\Delta t$) required to overcome the SHX loss so that the chiller produces cold.

$$\dot{Q}_e^{ce} = s \cdot \Delta\Delta t - \alpha \cdot \dot{Q}_{loss} = s \cdot (\Delta\Delta t - \Delta\Delta t_{min}) \tag{8}$$

$$\dot{Q}_g^{ce} = G \cdot [s \cdot (\Delta\Delta t - \Delta\Delta t_{min})] + \frac{s}{\alpha} \cdot \Delta\Delta t_{min} \tag{9}$$

$$COP_{ce} = \frac{\dot{Q}_e}{\dot{Q}_g} = \frac{\Delta\Delta t - \Delta\Delta t_{min}}{G \cdot (\Delta\Delta t - \Delta\Delta t_{min}) + \frac{\Delta\Delta t_{min}}{\alpha}} \tag{10}$$

With

$$s = \frac{1}{\frac{G}{UA_g z_g} + \frac{A}{UA_a z_a} + B \cdot \left(\frac{C}{UA_c z_c} + \frac{1}{UA_e z_e}\right)} \tag{11}$$

$$\alpha = \frac{\frac{1}{UA_g z_g} + \frac{1}{UA_a z_a}}{\frac{G}{UA_g z_g} + \frac{A}{UA_a z_a} + B \cdot \left(\frac{C}{UA_c z_c} + \frac{1}{UA_e z_e}\right)} \tag{12}$$

$$\Delta\Delta t_{min} = \frac{\alpha}{s} \cdot \dot{Q}_{loss} = \left(\frac{1}{UA_g z_g} + \frac{1}{UA_e z_e}\right) \cdot \dot{Q}_{loss} \tag{13}$$

Depending on the available information, the parameters of the CE can be determined from the machine design data or with the use of experimental operational results, as explained by Puig-Arnavat et al. [23]. The commonly expected deviation for this method on the cooling capacity is below 20% [23,24]. This is due to the fact that some important parameters are considered as constants (e.g., the arithmetic temperature difference correction factor, the internal enthalpies, the mass flow rates, the heat transfer coefficients, or $\Delta\Delta t_{min}$) while they are not [10,25,26]. Several improved models of the characteristic equation with better accuracy have been proposed to take into account the variation of different boundary conditions such as the mass flow rates or the exchanger design (absorber and generator) [12]. However, to date, the solution equilibrium deviation at the outlet of the sorption exchangers cannot be accounted for [27].

3.2. Adapted characteristic equation method and Carnot function model

The empirical methods do not require physical insight into the machine and are adapted to fit the experimental results. Consequently, they possess lower deviations compared with the CE method. Kühn and Ziegler [10] proposed the adapted CE method: an empirical method in which a multiple linear regression is performed to obtain an arbitrary characteristic temperature function ($\Delta\Delta t'$, Eq. (14)) that is linearly correlated to the cooling capacity (Eq. (15)). A second fit is then performed for the generator heat rate, a function of the $\Delta\Delta t'$, leading to Eq. (16). Kühn and Ziegler [10] used the external arithmetic mean temperatures of the generator, heat sink, and evaporator for the regression. However, in the present work, we propose the use of the inlet generator temperature, inlet heat sink temperature, and outlet evaporator temperature for the regressions (Eqs. (14)-(16)) as these variables are commonly used to characterize the part-load behavior of the absorption chillers (experimental prototypes and commercial machines).

$$\Delta\Delta t' = t_g^i - a \cdot t_{ac}^i + e \cdot t_e^o \tag{14}$$

$$\dot{Q}_e^{ce\prime} = s' \cdot \Delta\Delta t' + r = s' \cdot t_g^i - s' \cdot a \cdot t_{ac}^i + s' \cdot e \cdot t_e^o + r \tag{15}$$

$$\dot{Q}_g^{ce\prime} = b \cdot \Delta\Delta t' + c \tag{16}$$

The CFM is another empirical method described by Boudéhenn et al. [11]. This method has proven to estimate the experimental *COP* and cooling capacity ($\dot{Q}_e$) of different commercial machines operating with the same working pair (NH_3-H_2O) with a unique equation function of the machine's COP_{carnot} (shown in Eq. (17)) [11,16,28], in which ω_1, ω_2, τ_1, τ_2, and F_0 are fitted parameters to calculate either the machine's $\dot{Q}_e$ or its thermal *COP*.

$$F^{cfm} = \omega_1 \cdot e^{(-COP_{carnot}/\tau_1)} + \omega_2 \cdot e^{(-COP_{carnot}/\tau_2)} + F_0 \quad (17)$$

Both of the presented empirical models usually have an accuracy higher than 10% in cooling capacity [10,11,16,23], which is sufficient for being implemented as a control algorithm in absorption chillers. However, the underlying physical mechanisms of the machine operation are hidden [12].

3.3. Effectiveness model

A thermodynamic model based on the mass and energy balances of each component was developed using the thermodynamic properties of NH_3-$LiNO_3$ [29] and pure ammonia [30]. The presented model is able to account for the non-equilibrium conditions of the solution with the vapor phase at the inlet and the outlet of the sorption components (i.e., the absorber and generator) as it employs a thermal effectiveness and a mass effectiveness in each one. Moreover, the thermal and mass effectivenesses serve for the identification of the limiting components in the chiller and can then be used to optimize its thermal and electric performances. Finally, being a thermodynamic model, the different machine boundary conditions can be easily manipulated.

The state points (solid dots) in Figure 1 represent the calculated internal thermodynamic states of the NH_3-$LiNO_3$ solution (1–7), the NH_3 vapor (8 and 12), and the liquid NH_3 (9–11). Whereas the empty dots represent the external thermodynamic states of the driving source (t_g^i and t_g^o), the heat sink (t_{ac}^i and t_{ac}^o), and the chilled water source (t_e^i and t_e^o). The simplifying assumptions in the model are as follows:

- Heat losses are not taken into account.
- The expansion valves are isenthalpic and the pump is isentropic.
- The vapor at the output of the generator is considered to be in equilibrium with the solution concentration at point 3 and the high operating pressure [$T_8 = T_{eq}(P_h, x_3)$] [8].
- The refrigerant is at saturation state at the outlet of the condenser and the evaporator (points 9 and 12).

Most of the simulations in the literature make use of a thermal effectiveness or a global heat transfer coefficient for the sorption elements (i.e., the absorber and generator) and the solution is considered at equilibrium with the vapor phase under the operating pressure at their outlet [9]. However, this is never the case in real operating machines. Whenever the non-equilibrium conditions of the solution with the vapor phase at the inlet/outlet of the sorption elements are not taken into account, sensible heat effects are neglected [8]. Indeed, the sorption phenomenon involves a complex heat and mass transfer process in which the solution never makes use of its entire sorption potential. For this reason, the sorption elements are characterized by two types of effectiveness: a thermal and a mass effectiveness. The thermal effectiveness, also used for the other thermal components (considering isobaric condensation and evaporation processes), is defined as the ratio of the actual transferred heat to the maximum transferable heat (Eq. (18)). The mass effectiveness is defined as the ratio of the actual transferred mass to the maximum transferable mass (Eq. (19)).

$$\varepsilon_{th} = \frac{\dot{Q}}{\dot{Q}_{max}} \quad (18)$$

$$\varepsilon_m = \frac{\dot{m}_{sorp}}{\dot{m}_{sorp}^{max}} \quad (19)$$

In the case of the sorption exchangers, the two proposed types of effectiveness have been shown to be dependent on fewer parameters compared with heat/mass transfer coefficients [31] as they take into account the side of the exchanger that limits the transfers (solution or HTF side) and the state of the solution (subcooled or super-heated solution) at the inlet of the component to calculate the maximum transferable conditions. These conditions also depend on the HTF temperature deviation from the solution equilibrium conditions with the vapor phase. The more the HTF temperature deviates from the solution equilibrium temperature, the higher the absorption/desorption potential on the solution side. This gap is represented by the HTF equilibrium deviation temperature (Eq. (20)). If $\Delta T_{htf}^{eq} > 0$, the HTF has the potential to generate a desorption effect. Otherwise, the HTF induces an absorption process. On the other hand, the deviation of the solution from the equilibrium conditions with the vapor phase is represented by the solution equilibrium deviation temperature (Eq. (21)) [32]. If $\Delta T_{sol}^{eq} > 0$, the solution possesses a desorption potential, whereas if it is below 0, it possesses an absorption potential. In the following, only the case of the absorber will be discussed to explain the procedure followed in this work. A similar procedure is followed in the case of the generator.

$$\Delta T_{htf}^{eq,i/o} = t_{htf}^{i/o} - T_{eq}\left(P_v, x_{i/o}\right) \tag{20}$$

$$\Delta T_{sol}^{eq,i/o} = T_{sol}^{i/o} - T_{eq}\left(P_v, x_{i/o}\right) \tag{21}$$

The implemented absorber is a bubble-type absorber in counter-current configuration of the liquid phases (solution-HTF) and co-current configuration of the solution–vapor flow, as represented in Figure 2. The maximum absorbable mass depends on the solution flow rate and the potential of the HTF to cool it. This potential is represented by the equilibrium factor (Eq. (22)), defined as the ratio between the maximum heat that can be transferred to the HTF ($\dot{Q}_{htf,abs}^{max}$) to the maximum heat that can be transferred by the solution ($\dot{Q}_{sol,abs}^{max}$). The maximum amount of heat that can be transferred to the HTF in an infinitely long exchanger is proportional to the maximum enthalpy difference in the HTF itself when achieving an outlet temperature (t_{htf}^{o}) equal to the maximum temperature that the solution side can achieve (T_{sol}^{max}, Eq. (23)). When the inlet solution temperature is lower than the equilibrium solution temperature ($\Delta T_{sol}^{eq,i} < 0$), it has a tendency to absorb vapor (increase its temperature). Consequently, the maximum solution temperature corresponds to an adiabatic absorption in an infinitely long exchanger $T_{sol}^{max} = T_{sol}^{o,ad}$. $T_{sol}^{o,ad}$ is obtained through an iterative procedure in order to obtain the validity of Eqs. (26)-(28) and (25), with $\sum(\dot{Q}) = 0$ and $\sum(\dot{W}) = 0$ (the maximum absorbable mass, $\dot{m}_{abs}^{ad}$, to evaluate the mass effectiveness of an adiabatic absorber, is obtained with the same iterative procedure). If $\Delta T_{sol}^{eq,i} > 0$, it means that the solution enters the absorber in a super-heated state, in which case the solution would have a tendency to desorb vapor (decrease its temperature) and therefore, the maximum solution temperature would correspond to the inlet solution temperature itself ($T_{sol}^{max} = T_{sol}^{i}$). Finally, the maximum amount of heat that can be transferred by the solution ($\dot{Q}_{sol,abs}^{max}$) corresponds to an energy balance for an isothermal absorption in which the outlet solution temperature is equal to the inlet HTF temperature.

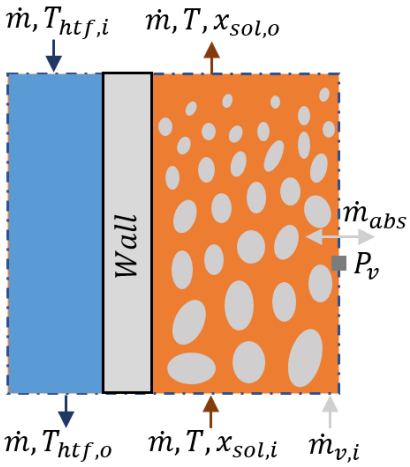

Figure 2. Control volume of the bubble absorber.

$$R_{abs} = \frac{\dot{Q}^{max}_{htf,abs}}{\dot{Q}^{max}_{sol,abs}} = \frac{\dot{m}_{htf}\left[h^{o}_{htf}(T^{max}_{sol}) - h^{i}_{htf}\right]}{\dot{m}^{i}_{sol}h^{i}_{sol} - \dot{m}^{o,iso}_{sol}h^{o,iso}_{sol}\left(t^{i}_{htf}; x^{o,iso}_{sol}\right) + \dot{m}^{iso}_{abs}h_{v}} \tag{22}$$

$$T^{max}_{sol} = \max[T^{i}_{sol}; T^{o,ad}_{sol}] \tag{23}$$

The maximum absorbable mass and transferable heat are obtained by solving the energy, mass, and species balances in the absorber using the maximum transferable heat depending on the limiting fluid. If $R>1$, then the solution is the limiting fluid and the maximum transferable heat corresponds to an isothermal absorption in an infinitely long absorber where the outlet solution temperature reaches the inlet HTF temperature (Eq. (24)), in which case $\dot{Q}^{max}_{abs} = \dot{Q}^{max}_{sol,abs}$ and $\dot{m}^{max}_{abs} = \dot{m}^{iso}_{abs}$. On the other hand, if $R<1$, the HTF is the limiting fluid and the maximum transferable conditions are achieved when it transfers its entire potential ($\dot{Q}^{max}_{abs} = \dot{Q}^{max}_{htf,abs}$) and the solution reaches equilibrium conditions with the vapor phase (Eq. (25)).

$$T^{o,iso}_{sol} = t^{i}_{htf} = T^{eq}_{sol}(P_{abs}; x^{o}_{sol}) \tag{24}$$

$$T^{o}_{sol}(h^{o}_{sol}; P_{abs}; x^{o}_{sol}) = T^{eq}_{sol}(P_{abs}; x^{o}_{sol}) \tag{25}$$

The simulation consisted of an iterative process in which the steady-state condition is reached when the condensed NH_3 vapor mass flow is equal to the evaporated vapor flow ($\dot{m}_8 = \dot{m}_{12}$). The mass and energy balances implemented for each component are described in Eqs. (26)–(28). Finally, the thermal coefficient of performance is defined by Eq. (29).

$$\sum \dot{m}_i = \sum \dot{m}_o \tag{26}$$

$$\sum(\dot{m}_i x_i) = \sum(\dot{m}_o x_o) \tag{27}$$

$$\sum((\dot{m}_i h_i) - (\dot{m}_o h_o)) + \sum(\dot{Q}) + \sum(\dot{W}) = 0 \tag{28}$$

$$COP_{th} = \frac{\dot{Q}_e}{\dot{Q}_g} \tag{29}$$

4. Results and validation of the models

In the following sections, the implementation of the different approaches presented in Section 3 to the 10-kW NH_3-$LiNO_3$ water-cooled absorption chiller is presented. As mentioned before, the COP_{carnot} was used as a variable to represent the results from the different models as well as the experimental results, in which case the CFM was used to show the trend of the latter.

4.1. Characteristic equation method

Ochoa and Coronas [20] presented the CE (Section 3.1) of the studied absorption chiller and obtained the coefficients presented in Table 4. The values of the heat rates (in the generator and the evaporator) and thermal COP are compared with the experimental results (Table 2) in Figure 3a. The deviations in the cooling capacity remain below 15%, with the exception of two cases. On the other hand, the generator heat rate correlation presents deviations of less than 10%, with the exception of one operating condition.

In the CE (Figure 3a), the cooling and generator heat rates are linearly dependent on $\Delta\Delta t$ (Eqs. (8) and (9)). An increase in the generator (t_g^{avg}) or evaporator (t_e^{avg}) temperatures increases $\Delta\Delta t$ (Eq. (7)); hence $\dot{Q}_e$ and $\dot{Q}_g$ also increase, whereas an increase in the heat sink temperature (t_{ac}^{avg}) has the opposite effect. These average external temperatures at the three levels have almost the same influence on $\Delta\Delta t$ (the "temperature lift" terms, t_c^{avg} and t_e^{avg}, being corrected by a Dühring coefficient (B) that is close to 1 (1.18 in this case); hence their variation has almost the same impact on $\dot{Q}_e$ and $\dot{Q}_g$. This generates an important data dispersion that is especially noticeable on the experimental COP at low $\Delta\Delta t$ values due to a stronger influence of the intermediate (heat dissipation) temperature that is not taken into account in the $\Delta\Delta t$ term [10,23]. Another factor that influences the data dispersion is the simplifying assumption of fundamental parameters (e.g., the heat transfer regimes or internal/external irreversibilities) as constants, as discussed in Section 3.1, which leads to functions with constant slopes and intersects [10,25,26]. Finally, the assumption of the solution being at equilibrium with the vapor phase at the outlet of the sorption components is another hypothesis that is not valid in real operating conditions, and it might add imprecision to the estimated results.

The representation of the characteristic equation results with the COP_{carnot} domain is shown in Figure 3b. The trend followed by the experimental results with the COP_{carnot} is shown by the CFM (Eq. (17), Table 5, and dashed lines in Figure 3b), with deviations that remain below 10% for most of the cases. In this representation of the absorption chiller, the assumption of a linear dependence between the generator and evaporator heat rates with the external temperatures is not used. Different from the $\Delta\Delta t$ term, in the COP_{carnot} the weight of each temperature is not linear. From Eq. (1) and the external temperature conditions studied in the present work (Table 1), it is evident that the one with the highest impact is the heat sink temperature (t_{ac}^i, especially at low COP_{carnot}), followed by the chilled water temperature (t_e^o, especially at high COP_{carnot}) and the inlet hot water temperature (t_g^i, especially at low COP_{carnot}), respectively. This distribution of the HTF temperatures effect seems to better represent the machine's operating regime as there is a noticeable lower experimental COP dispersion (a CFM average deviation of 1.96% compared with 4.1% for the CE method), especially for two cases (tests 13 and 14, green dots in Figure 3) in which the experimental results were situated at a lower regime in the COP_{carnot} domain due to a dominance of t_{ac}^i over t_g^i. In this representation, the evaporator and generator loads rapidly increase at low COP_{carnot} regimes, with a slope that decreases approaching an asymptote at high regimes, stabilizing the COP. Furthermore, the trends followed by the CE method and the CFM diverge considerably.

Table 3. Coefficients of the characteristic equation [20].

Coefficient	Value
s (kW K^{-1})	0.52
α (-)	0.29
G (-)	1.27
$\Delta\Delta t_{min}$ (K)	2.75
B (-)	1.18

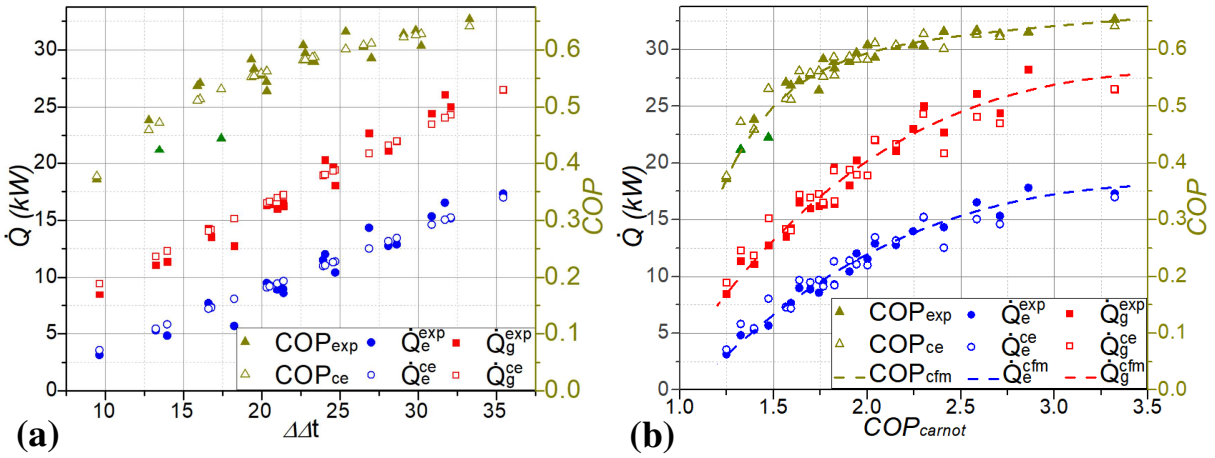

Figure 3. Results of the characteristic equation method vs. experimental results represented in the (a) ΔΔt domain and in the (b) COP_{carnot} domain.

4.2. Adapted characteristic equation method and Carnot function model

The least squares method along with the generalized reduced gradient (GRG) nonlinear method of the Excel Solver were used to fit the parameters of the equations presented in Section 3.2 to the data of Table 2. The fitted parameters of the adapted CE method are presented in Table 4, whereas those of the CFM are presented in Table 5. With the adapted CE method, the adapted characteristic temperature difference, *ΔΔt'* (Eq. (14)), is used to represent the functioning of the machine. This fitted parameter was proposed to better divide the effects of external temperatures [10]. Different from the COP_{carnot}, the external temperatures possess a constant influence on *ΔΔt'* (factors 1, *a*, and *e* for t_g^i, t_{ac}^i, and t_e^o in Eq. (14), respectively). However, in the present study, similar to the COP_{carnot}, the heat sink temperature (t_{ac}^i) possesses the highest influence (a = 2.773), followed by the chilled water temperature (e = 1.88) and the heat source temperature, respectively.

The adapted characteristic loads (generator and evaporator) and COP are compared with the experimental results in the COP_{carnot} domain in Figure 4. The correlated results present considerably lower deviations compared with the conventional CE, showing deviations below 10% for most of the cases, with the exception of two conditions. However, in spite of the good model estimations, a physical understanding of the machine operation cannot be inferred. Therefore, it is not reliable to identify deviations from normal machine operating conditions, systematic deviations, or the limiting components in the system, for which models with a physical basis are required [12].

Both methods (the adapted CE method and the CFM), being regressions of the experimental dataset, are in good agreement; the CFM has less experimental COP dispersion (an average deviation of 1.96% versus 2.68% for the adapted CE method). The two empirical methods possess a deviation below 10% for most of the cases. Nevertheless, the CFM is based on a parameter (the COP_{carnot}) that has a thermodynamic basis and that does not depend on the specific machine's characteristics or experimental dataset; therefore, it can be employed for any machine or modeling method, which gives it an advantage over the adapted CE method. The COP_{carnot} thus seems to be a reliable parameter with which to represent the entire range of the machine operating conditions.

Table 4. Coefficients of the adapted characteristic equation.

Coefficient	Value
s'	0.373
a	2.773
e	1.88
r	4.716
b	0.489
c	10.691

Table 5. Coefficients of the Carnot function model for the cooling capacity and COP.

	$\dot{Q}_e^{cfm}$ (kW)	COP^{cfm}
ω_1	159.56	-0.44
ω_2	-172.09	-10.57
τ_1	4.59	13.14
τ_2	2.46	0.32
F_0	-14.93	0.99

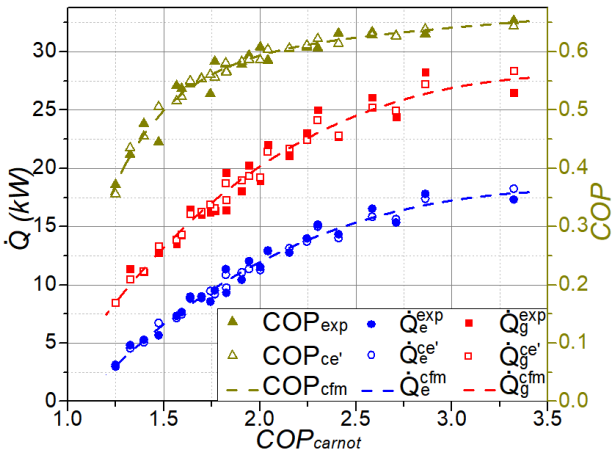

Figure 4 Results of the adapted characteristic equation method vs. experimental results in the COP_{carnot} domain.

4.3. Effectiveness model

In the present section, the results from the modeling of the absorption chiller using its thermal and mass effectivenesses are presented. First, the different thermal and mass effectivenesses of the system components are obtained for the whole range of tested conditions, which allows for the identification of the limiting components. The present work proposes the use of the Carnot function model (Eq. (17)), which to date was used exclusively to estimate the absorption chiller cooling capacity and thermal COP, as a simple equation to represent the variable exchangers effectivenesses as a function of the COP_{carnot}. Second, the modeling results of the thermal loads and COP are presented and discussed.

4.3.1 Thermal and mass effectivenesses of the components

In order to calculate the thermal effectiveness of the evaporator, the internal pressure data were used to obtain the internal saturation temperature conditions using the correlations of [30] and considering an isobaric evaporation process. These data, however, were available for a series of experiments in a shorter cooling capacity range (3.1–12 kW) than the total number of tests. The temperature measurement ranges and operating conditions and their uncertainties are presented in Table 5. The experimental results and a correlation (see Table 8) with a limit at an effectiveness of 0.7 were plotted against the COP_{carnot} (Figure 5). The evaporator effectiveness decreases at very low cooling capacities due to the nature of the exchanger, which is a flooded evaporator whose refrigerant level is controlled by an electronic expansion valve [13]. The fact that the proposed correlation is out of the uncertainty range in some experimental conditions has no physical sense and is attributed to other factors during experimentation. Indeed, as the evaporating load increases, the refrigerant level in the evaporator rises, increasing the heat exchange area. This, together with the confined pool boiling enhancement present for the studied conditions (capillary length of ammonia in the same range as the space between plates of 2 mm) [33], should increase the thermal effectiveness of the exchanger, achieving a maximum value of approximately 0.7.

Table 6. Evaporator internal and external operating temperatures.

Variable	Measurement range	Uncertainty
t_e^i (°C)	8.9-18.4	±0.1 °C
t_e^o (°C)	8; 15	±0.1 °C
T_e^{sat} (°C)	6.32-14.2	±0.3 °C

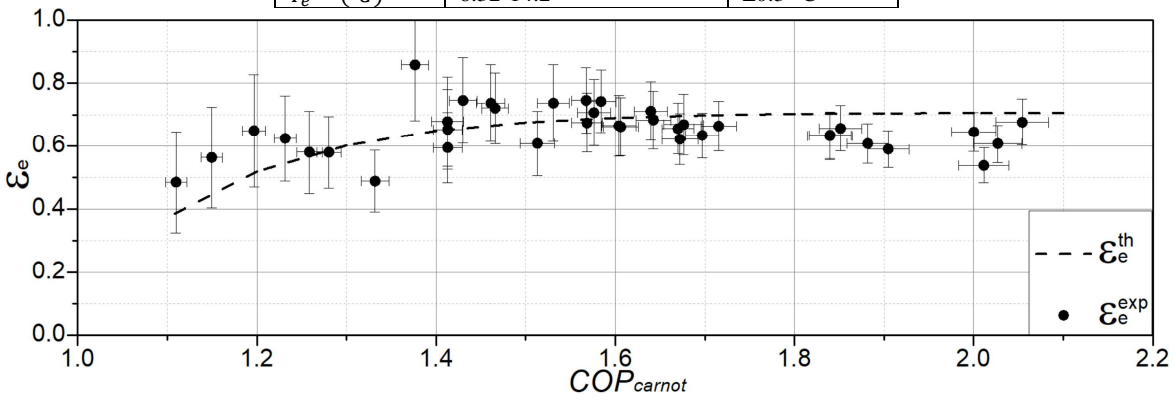

Figure 5. Evaporator thermal effectiveness against COP_{carnot}.

The operating conditions of the condenser are shown in Table 6. In this case, as there is no direct temperature measurement at the outlet of the exchanger, t_c^o can be approximated by energy balances at the evaporator and condenser. Unfortunately, the effectiveness uncertainties of this calculation are too large and lead to condenser effectiveness greater than 1. Therefore, the theoretical effectiveness for the nominal operating conditions of the condenser was determined by means of the number of transfer units (NTU) [34] calculated from the convection thermal resistance on the water side, the stainless steel wall conduction thermal resistance, and the conduction thermal resistance of the NH_3 refrigerant falling film in the conditions of the highest film thickness. These calculations led to a global heat transfer coefficient of at least 2683 W m^{-2} K^{-1}, an NUT of at least 5.49, and a thermal condenser effectiveness of at least 0.989, showing that the condenser is not a limiting component in the system, which is in agreement with the over-dimensioning of 86% for its nominal conditions [13]. Therefore, a constant condenser effectiveness of 0.99 was used for the simulations.

Table 7. Condenser internal and external temperature operating conditions.

Variable	Measurement range	Uncertainty
t_c^i (°C)	32.6-44	±0.1 °C
t_c^o (°C)	Not measured	-
T_c^{sat} (°C)	36-46	±0.4 °C

The sorption exchangers were characterized be their thermal and mass effectivenesses using the experimental results of Amaris Castilla [35] and Zacarías Santiago [36] for their plate heat exchangers operating as absorber and generator, respectively. In the nominal conditions of the machine, represented by solid dots in Figure 6, the values of the effectivenesses are as follows: $\varepsilon_a^m = 0.479, \varepsilon_a^{th} = 0.492, \varepsilon_g^m = 0.629, and\ \varepsilon_g^{th} = 0.642$. In order to investigate the evolution of the effectivenesses for the range of COP_{carnot} studied, a program was run to identify the values of the corresponding thermal and mass effectivenesses that would lead to the experimental cooling capacity. Considering that both the absorber and generator are bubble plate heat exchangers, the evolution of the effectivenesses in both exchangers was considered to follow the same trend, i.e., the same correlation factor (*f*) is multiplied by the nominal absorber/generator effectivenesses at each COP_{carnot} condition. A correlation with the form of Eq. (17) was then obtained from the scattered results to give the functions of the absorber and generator effectivenesses (see Figure 6 and Table 8). Figure 6 shows the evolution of all the thermal and mass effectivenesses of the exchangers. An increase in the absorber and generator effectivenesses can be observed while increasing the COP_{carnot}. This can be explained by

the fact that both operate in a bubble regime, and while increasing the cooling load, the bubble presence is progressively more common, generating instabilities in the solution flow and increasing the exchanger effectiveness. The effectivenesses will be discussed in more detail in Section 5.5. The generator/absorber thermal effectiveness and mass effectiveness calculated by the proposed correlation are in accordance with the experimental effectivenesses calculated under nominal conditions at a COP_{carnot} of 1.85 (solid dots in Figure 5) (a deviation of less than 4%).

Finally, even though the solution heat exchanger was designed for a nominal thermal effectiveness of 0.9 [13], no experimental data were available to support this value. Instead, a good agreement with the experimental results was found to occur at an SHX effectiveness of 0.65. Besides a possible experimental effectiveness lower than the nominal design value, other factors such as the non-idealities that were not taken into account (e.g., no heat losses to the environment or the variations in the solution mass flow rate) that lead to a lower machine performance might be reflected in this effectiveness. Therefore, this value was used as the SHX thermal effectiveness and kept as constant for the entire range of operating conditions since the available information does not allow us to estimate a variable behavior.

While the simulation methods usually consider a constant heat transfer coefficient (constant effectiveness) in the absorption chiller components for the entire range of operating conditions, it can be observed in Figure 6 that there are some exchangers for which the effectivenesses decrease noticeably at low cooling loads. The absorber is clearly the most limiting component in the system, probably due to the high viscosities and low mass diffusivity values of the solution that operates at lower temperatures compared with the generator [37]. Indeed, some studies have reported lower than expected performances of the NH_3-$LiNO_3$ working fluid in sorption exchangers, which has been attributed to its elevated viscosity [5]. The evaporator also seems to be a limiting component due to a refrigerant level control that can be optimized by a variable chilled water flow rate, which would also have a positive impact on the total electric COP of the chiller. Moreover, its maximum effectiveness can be increased by increasing the length or the number of plates in the exchanger, at the cost of a depreciated system compactness. The same applies to the SHX and sorption exchangers, for which an increase in the number of plates or exchanger length would increase the solution residence time in the exchanger, improving its effectiveness.

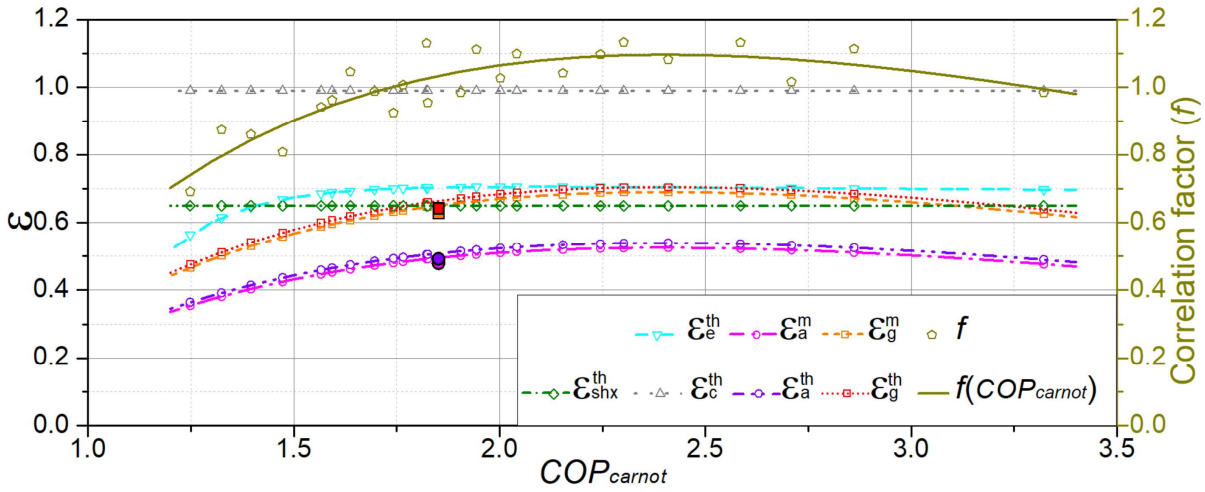

Figure 6. Thermal and mass effectivenesses correlations of the exchanger components and correlation factor of the sorption exchangers (solid dots for the nominal experimental effectivenesses values).

Table 8. Thermal and mass effectivenesses correlations of the system components for the range of $COP_{carnot} \in [1.2:3.4]$.

Component	Thermal effectiveness	Mass effectiveness
Evaporator	$\varepsilon_e^{th} = 0.5 \cdot e^{(-COP_{carnot}/61)} - 155 \cdot e^{(-COP_{carnot}/0.18)} + 0.23$	-
Condenser	$\varepsilon_c^{th} = 0.99$	-
Solution heat exchanger	$\varepsilon_{shx}^{th} = 0.7$	-
Absorber*	$\varepsilon_a^{th} = 0.492 \cdot f(COP_{carnot})$	$\varepsilon_a^{m} = 0.479 \cdot f(COP_{carnot})$
Generator*	$\varepsilon_g^{th} = 0.642 \cdot f(COP_{carnot})$	$\varepsilon_g^{th} = 0.629 \cdot f(COP_{carnot})$

$$* f(COP_{carnot}) = 4.36 \cdot e^{(-COP_{carnot}/9.18)} - 4.16 \cdot e^{(-COP_{carnot}/0.98)} - 1.9$$

4.3.2 Effectiveness model validation

The correlations provided in Table 8 and shown in Figure 6 for the thermal and mass effectivenesses of the components were implemented in the EM and the results obtained are shown in Figure 7. Most of the simulated results present deviations below 10% compared with the experimental results. The simulated cooling capacity follows the same trend as the experimental one, in close agreement with the CFM. On the other hand, the simulated generator heat rate, although in close agreement in most of the operating conditions, diverges somewhat at the lower COP_{carnot} values. This also has an impact on the simulated COP, which is higher than the experimental COP at low COP_{carnot} values. This divergence might be due to factors that were not taken into account as the variation of the SHX effectiveness in real operating conditions and heat losses to the environment. The model presented here, which is able to identify the internal non-equilibrium conditions of the solution with the vapor phase at any point, is used as a tool to better explain the behavior of the machine in the following.

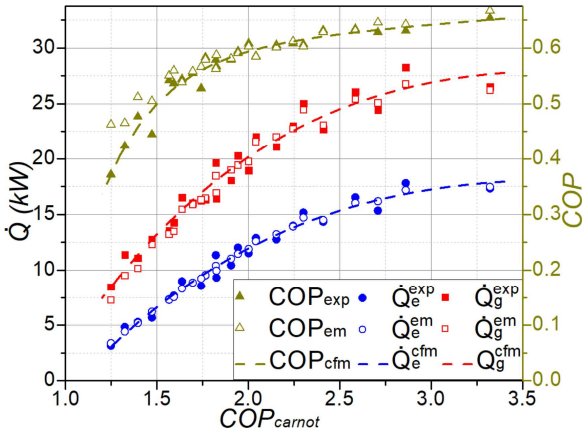

Figure 7. Results of the effectiveness method vs. experimental results in the COP_{carnot} *domain.*

5. Discussion of the internal operating conditions through the effectiveness model

During the machine operation, the high pressure and low pressure are mainly controlled by the heat sink temperature and the chilled water temperature, respectively. Owing to the decrease in the heat sink temperature for high COP_{carnot} values, the high pressure (P_h) is reduced as well, decreasing the solution saturation temperature conditions in the generator, thereby enhancing the desorption phenomenon for a given heat source temperature. On the other hand, higher chilled water temperatures lead to greater low pressures (P_l) at high COP_{carnot} values, increasing the solution saturation temperature conditions, which is favorable for the absorption phenomenon at a given heat sink temperature. The following sections discuss the internal operating conditions of the machine. This better understanding allows for the identification of opportunities to improve thermal and electric COPs.

5.1 Solution concentration conditions

Figure 8 shows the internal solution concentrations (concentrated and diluted side) and the concentration difference (right axis). The concentrated side corresponds to the outlet concentration of the generator and the inlet concentration of the absorber and vice versa for the diluted side. These concentrations, result of all the heat and mass transfer phenomena in the machine, are of great importance since they have a direct impact on the solution thermophysical properties, which control the performance of the exchangers in the system. High absorber and generator temperatures lead to higher concentrations, whereas the evaporator and condenser temperatures have the opposite effect.

As COP_{carnot} increases, the refrigerant flow in the machine increases, proportionally increasing the concentration differences (Δx) between the inlet and outlet of the sorption components. In the entire range of operating conditions, the mass fraction on the concentrated side remained moderately stable with values between 0.5 and 0.536. As the cooling capacity increases, the diluted-side concentration decreases with values ranging from 0.512 to 0.435. The impact of the intermediate temperature is not the same on the generator as on the absorber. Whereas the outlet absorber mass fraction seems highly impacted by the intermediate temperature source that decreases with the COP_{carnot}, the outlet generator mass fraction does not follow the same trend. This is mostly due to the higher generator effectivenesses compared with those of the absorber (see Figure 6) and the enhanced desorption potential due to a decrease in the high operating pressure (owing to the reduction of the intermediate temperature source with the COP_{carnot}).

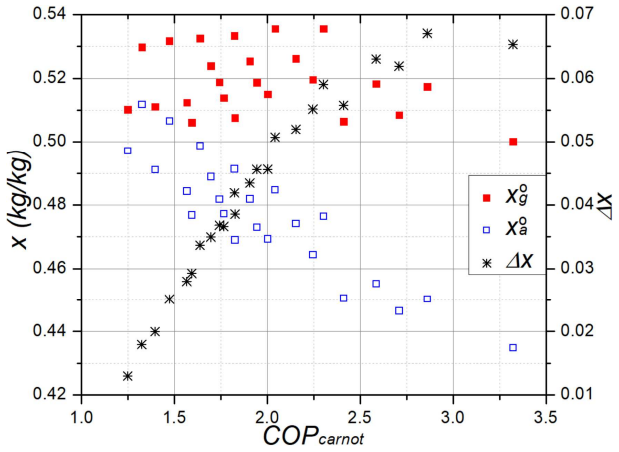

Figure 8. Simulated machine internal solution concentrations and concentration differences at part-load operation.

5.2 Equilibrium factor

Figure 9 shows the equilibrium factor (R, Eq. (22)) in the absorber and the generator for each operating condition. As mentioned before, this parameter represents the HTF potential to heat/cool down the solution. When R>1, the maximum transferable heat and mass are limited by the solution flow conditions. As the cooling capacity increases, the equilibrium factors decrease. This happens because as the equilibrium conditions in the machine change, the heat transfer fluids deviate from them (Figure 11a), increasing the absorption/desorption potential of the solution, and decreasing the equilibrium factor. One mark is outside the trend in the absorber (COP_{carnot}=2.41 in Figure 9) due to an uncommon low heat sink flow rate in test 7 (Table 2), which decreases the HTF cooling potential and therefore the equilibrium factor.

While the solution side is the one limiting the sorption phenomena (R>1), an increase in the HTF flow rate only leads to a decrease in the machine's electric COP (the absorber/generator effectivenesses are not substantially improved), as observed in [31]. Consequently, for an optimal electric COP, operation at equilibrium factors close to 1 is desirable. Figure 9 shows the great potential of COP_{elect} improvement by a reduction in the HTF mass flow rates of up to 4–5 times at low COP_{carnot} values and approximately 2 times at high cooling regimes. Regarding the phase-change exchangers, the external

condenser flow rate can also be reduced as it operates with an effectiveness close to 1, whereas the chilled water mass flow rate can be reduced at low cooling regimes to increase the thermal effectiveness of the evaporator, as mentioned in Section 4.3.1. A proper control of the external HTFs might subsequently lead to important improvements in the electric *COP*, which was a major concern during the machine development [38].

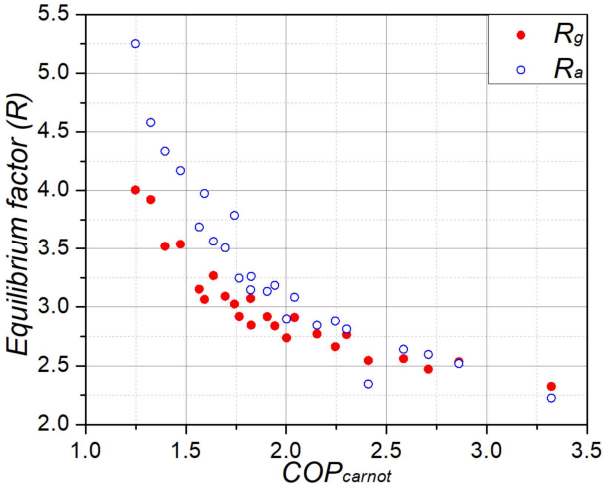

Figure 9. Equilibrium factor for the sorption components (absorber and generator) in the different tested conditions.

5.3 Solution flow conditions

The analysis of the solution flow conditions in the sorption exchangers is of fundamental importance as it is the one that limits the transfers in the tested conditions (R>1 from Figure 9). Figure 10 shows that the chilled water temperature is a dominant factor in the kinematic viscosity, volumetric flow rate, and therefore in the solution Reynolds number. Lower chilled water temperatures lead to higher viscosities due to the higher solution concentrations caused by a decreased absorption potential. Regarding the absorber, for each chilled water temperature, as the COP_{carnot} increases, the heat sink temperature decreases, lowering the solution absorber temperature, whereas the generator temperature increases, slightly increasing the solution concentration, and both phenomena increase the inlet viscosity of the solution in the absorber (Figure 10a), this variation being less noticeable at high COP_{carnot} values due to a lower concentration variation in the concentrated solution side (Figure 8). On the other hand, in the case of the generator, the viscosity for each evaporator temperature decreases with the COP_{carnot} mainly via the decrease in the concentration of the diluted solution side. From Figure 10a, the difference in the operating solution viscosity range between the absorber and the generator is clear, which is one of the reasons why the absorber has lower performance compared with the generator (Figure 6) [37].

Figure 10b shows the evolution of the inlet solution volumetric flow rate ($\dot{V}$) and the Reynolds number (Re) in the absorber and the generator. Besides the kinematic viscosity, the volumetric flow rate also has a direct impact on Re. Despite a constant solution mass flow rate, due to a decrease in the density at the inlet of the generator, the volumetric flow rate increases with COP_{carnot}. On the other side, $\dot{V}_a^i$ decreases with COP_{carnot} due to the decrease in the solution mass flow rate (higher refrigerant desorption at the generator). The variations in the solution kinematic viscosities and volumetric flow rates lead to an increase in Re at the generator and vice versa at the absorber.

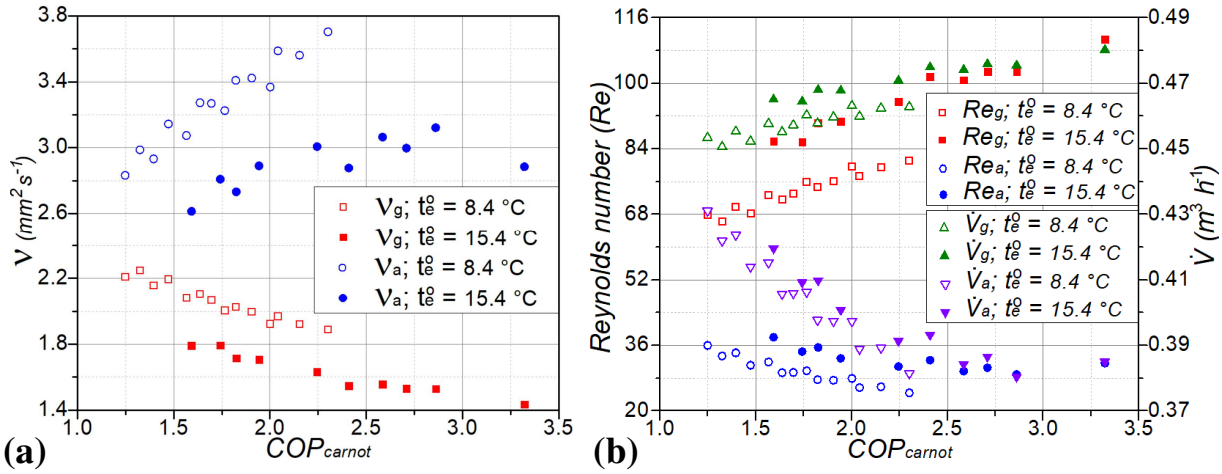

Figure 10. Inlet solution conditions in the absorber and generator. (a) Dynamic viscosity and (b) Reynolds number.

5.4 Equilibrium deviation temperatures

Figure 11 shows the HTF equilibrium deviation temperatures (Eq. (20)) at the inlet of the sorption components and the solution equilibrium deviation temperatures (Eq. (21)) at their inlet/outlet. According to Figure 11a, as the COP_{carnot} increases, the HTF in the absorber and the generator increase their deviation from the solution equilibrium conditions (with the vapor phase), increasing the sorption potential on the solution side and therefore, increasing the machine's cooling capacity. From Figure 11b, contrary to the standard assumption in the modeling of absorption chillers, it is clear that the solution is rarely in equilibrium conditions (with the vapor phase) at the outlet of the sorption elements. The low evaporating pressures and high absorber temperatures at low COP_{carnot} increase the deviation from the equilibrium conditions of the solution at the inlet of the absorber. As the COP_{carnot} increases, the absorber temperature decreases and the operating pressure increases, which decreases the solution equilibrium deviation temperature until reaching a value of approximately 5°C. The $\Delta T_{sol}^{eq,o}$ reaches values of approximately 2.5°C at the absorber at high COP_{carnot}. A similar behavior is observed at the generator inlet, for which the solution arrives highly subcooled at low cooling regimes. In these conditions, vapor is generated at the interface between the solution flow and the plate. The evaporation induces mass diffusion close to the interface and locally modifies the equilibrium temperature. The high concentration gradient induced in the solution flow (low mass diffusivity) seems to explain the average subcooling of the solution at the outlet of the component despite the clear vapor generation. This subcooled boling phenomenon, also reported in [39], is similar to the one observed in convective boiling of subcooled liquids [40]. The decrease in the solution concentration at the generator inlet for high COP_{carnot} values (Figure 8) brings the solution closer to the equilibrium conditions (with the vapor phase) at the inlet of this component. This solution reaches a super-heated state at the outlet of the generator at high cooling regimes (high COP_{carnot}), showing the desorption potential that was unused owing to its limited thermal and mass effectivenesses.

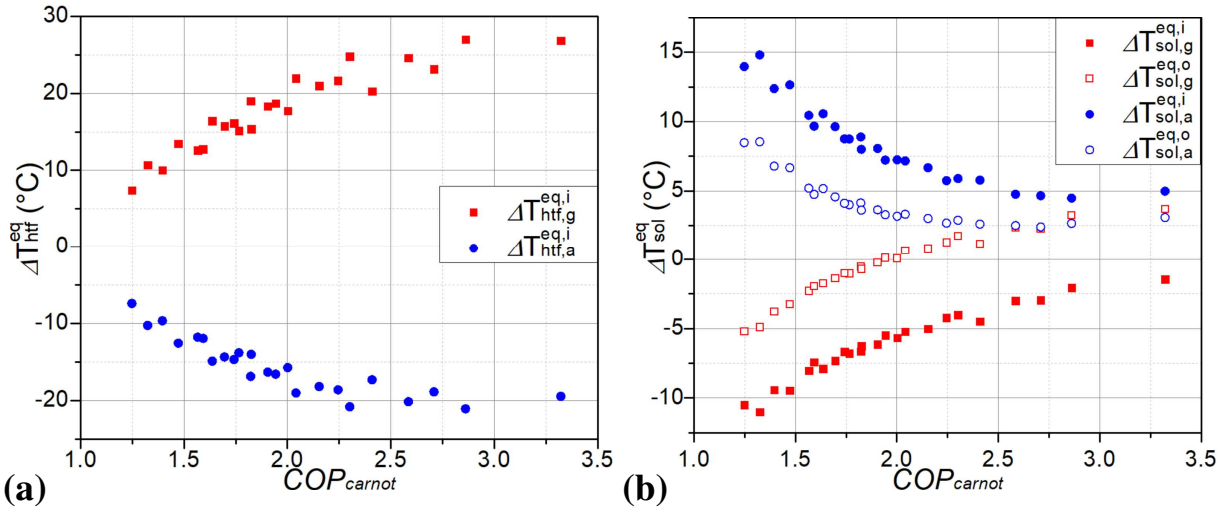

Figure 11. Temperature deviation from the internal solution equilibrium conditions of the (a) heat transfer fluid and the (b) solution.

5.5 Thermal and mass effectivenesses of the sorption exchangers

Different factors exist that impact the absorber/generator thermal and mass effectivenesses. In an operation in which the solution limits the transfers (R>1), the solution flow conditions and its deviations from equilibrium (with the vapor phase) are of fundamental importance. Regarding the solution flow conditions (Figure 10), both sorption exchangers present opposite effects. Indeed, a decreasing viscosity in the generator (Figure 10a) increases the exchanger performance due to enhanced bubble hydrodynamic disturbance effects, whereas an increased volumetric flow rate (Figure 10b) increases the solution velocity at the inlet of the exchanger, decreasing the solution residence time and therefore decreasing the exchanger performance. The same happens in the absorber but with opposite phenomena.

Considering that the viscosity effects are somewhat balanced by the change in the solution volumetric flow rates, the variation in the sorption effectivenesses might then be controlled by the solution equilibrium deviations. Indeed, a high subcooling of the solution at the inlet of the generator and a high super-heating at the inlet of the absorber (Figure 11b) are in agreement with the low effectivenesses of the sorption exchangers at low COP_{carnot} values (Figure 6). However, their approach to the equilibrium while increasing the COP_{carnot} is congruent with the increase in the effectivenesses. Another factor that might lead to an increase in the effectivenesses at higher COP_{carnot} values is the variation in the solution concentrations, especially at the inlet of the desorber (see Figure 8). Lower solution concentrations lead to a lower viscosity and higher performances. Furthermore, the slight reduction in the absorber/generator effectivenesses at high COP_{carnot} (Figure 6) might be the result of other factors (e.g., heat losses to the environment). A more detailed experimental study is required to determine the predominant parameter in the effectivenesses of the sorption exchangers and to more precisely characterize their evolution during the different operating regimes. It seems that the solution deviation from equilibrium conditions (with the vapor phase) has a stronger impact on the mass effectiveness than on the thermal effectiveness [31].

6. Conclusion

The characterization of a 10-kW water-cooled absorption chiller was performed by means of four different methods that use the external fluid temperatures to situate the machine operating conditions: the CE method (semi-empirical), the adapted CE method and the CFM (both empirical), and a thermodynamic model (physical), called the effectiveness model (EM), based on thermal and mass effectivenesses. The COP_{carnot} was used as a common parameter to represent the different operating conditions of the chiller and situate the different modeling results. When no information about the internal working fluid conditions is required and an extensive database of experimental results is

available, the empirical models offer a simple tool to calculate the cooling power and thermal COP of the system. On the other hand, if the number of experimental results is limited but the machine components design data is available, the CE method is a viable option. Finally, if information about the thermal and mass effectivenesses of the internal components is available in the range of studied conditions, the proposed EM can be employed to identify the limiting components in the system and analyze at any time the internal non-equilibrium conditions of the solution with the vapor phase. Furthermore, in the present study, it allowed us to identify COP_{elect} improvement opportunities since the HTF flow rates in all the components can be reduced, especially at low cooling regimes.

The thermal and mass effectivenesses are parameters that, different from the heat/mass transfer coefficients/fluxes, depend on fewer boundary conditions and consider the non-saturated conditions at the inlet and the outlet of the components. Therefore, they can be used to create more complete models to characterize the part-load behavior of absorption chillers (internal and external thermodynamic states) and identify optimization opportunities for each individual component, or be applied in dynamic models for the study of systems in constantly changing conditions (e.g., while using solar thermal energy or ambient temperature as heat sources). Nevertheless, more detailed experimental studies are required to better characterize the variations of the different effectivenesses as functions of the COP_{carnot} of the chiller in real machine operating conditions.

Acknowledgments

The authors would like to thank the Mexican sectorial fund "CONACYT-SENER-SUSTENTABILIDAD ENERGÉTICA" and the InnoEnergy PhD School Programme of the European Institute of Technology (EIT) for their support of this research.

References

[1] IEA, The Future of Cooling, Paris, France, 2018. https://www.iea.org/reports/the-future-of-cooling.

[2] X.G. Casals, Solar absorption cooling in Spain: Perspectives and outcomes from the simulation of recent installations, Renew. Energy. 31 (2006) 1371–1389. https://doi.org/10.1016/j.renene.2005.07.002.

[3] E. Dube, A. Cha, O.P. Agboola, J. Or, A.H. Fakeeha, A.S. Al-fatesh, Energetic and exergetic analysis of solar-powered lithium bromide- water absorption cooling system, J. Clean. Prod. 151 (2017) 60–73. https://doi.org/10.1016/j.jclepro.2017.03.060.

[4] M.R. Ally, V. Sharma, O. Abdelaziz, Exergy analysis of electrically- and thermally-driven engines to drive heat pumps: An exhaustive comparative study, Int. J. Refrig. 76 (2017) 313–327. https://doi.org/10.1016/j.ijrefrig.2017.02.011.

[5] A. Altamirano, B. Stutz, N. Le Pierrès, Review of small-capacity single-stage continuous absorption systems operating on binary working fluids for cooling: Compact exchanger technologies, Int. J. Refrig. 114 (2020) 118–147. https://doi.org/10.1016/j.ijrefrig.2020.02.033.

[6] J. Sjöberg, Q. Zhang, L. Ljung, A. Benveniste, B. Delyon, P.Y. Glorennec, H. Hjalmarsson, A. Juditsky, Nonlinear black-box modeling in system identification: a unified overview, Automatica. 31 (1995) 1691–1724. https://doi.org/10.1016/0005-1098(95)00120-8.

[7] J. Labus, J.C. Bruno, A. Coronas, Performance analysis of small capacity absorption chillers by using different modeling methods, Appl. Therm. Eng. 58 (2013) 305–313. https://doi.org/10.1016/j.applthermaleng.2013.04.032.

[8] K. Herold, R. Rademacher, S. Klein, Absorbtion Chillers and Heat Pumps, 2nd ed., CRC Press, Taylor & Francis Group, Boca Raton, FL, 2016.

[9] M. Aiane, J. Ramousse, B. Stutz, M. Bouyaud, E. Boudard, Dynamic Modeling Of An

Automotive Air-Conditioning System By Absorption, in: Int. Sorption Heat Pump Conf. August 7-10, Tokyo, Japan, 2017.

[10] A. Kühn, F. Ziegler, Operational results of a 10kW absorption chiller and adaptation of the characteristic equation., in: First Int. Conf. Sol. Air Cond. Oct. 6-7, Bad-Staffelstein, Germany, 2005.

[11] F. Boudéhenn, S. Bonnot, H. Demasles, A. Lazrak, Comparison of different modeling methods for a single effect water-lithium bromide absorption chiller, in: Int. Conf. Sol. Energy Build. Sept. 16-19, Aix-les-Bains, France, 2014.

[12] O. Buchin, J. Albers, F. Ziegler, Review of regression models for absorption heat pumps, in: Heat Powered Cycles Conf. June 27-29, Nottingham, UK, 2016.

[13] M. Zamora, Industrial Optimization and Control Strategy of an Air-cooled Ammonia/lithium Nitrate Absorption Chiller (in Spanish), PhD Universitat Rovira i Virgili, 2012. https://www.tdx.cat/handle/10803/284083.

[14] M. Bourouis, A. Coronas, M. Vallès, M. Zamora, Air/Water or Water/Water Absorption Water Cooler Using Ammonia and Lithium Nitrate, Patent No.: WO2011039397A1, 2011.

[15] A. Altamirano, N. Le Pierrès, B. Stutz, Review of small-capacity single-stage continuous absorption systems operating on binary working fluids for cooling: Theoretical, experimental and commercial cycles, Int. J. Refrig. 106 (2019) 350–373. https://doi.org/10.1016/j.ijrefrig.2019.06.033.

[16] F. Boudéhenn, S. Bonnot, H. Demasles, F. Lefrançois, M. Perier-Muzet, D. Triché, Development and Performances Overview of Ammonia-water Absorption Chillers with Cooling Capacities from 5 to 100 kW, Energy Procedia. 91 (2016) 707–716. https://doi.org/10.1016/j.egypro.2016.06.234.

[17] F. Ziegler, Sorptionswärmepumpen (in German), Forschungsberichte Des Dtsch. Kälte- Und Klimatechnischen Vereins e.V., Nr. 57, DKV, Stuttgart. (1998).

[18] H.M. Hellmann, C. Schweigler, F. Ziegler, The characteristic equations of absorption chillers, in: Int. Sorption Heat Pump Conf. March 24-26, Munich, Germany, 1999.

[19] U. Jakob, Investigations into solar powered diffusion-absorption cooling machines, PhD Montfort University Leicester, 2005.

[20] A.A. V Ochoa, A. Coronas, Aplicação do método da equação característica num chiller por absorção com NH3/LiNO3, in: VI Congr. Ibero-Americano Ciências e Técnicas Do Frio, May 3-6, Coimbra, Portugal, 2016.

[21] H.M. Hellmann, F. Ziegler, Simple absorption heat pump modules for system simulation programs, ASHRAE Trans. 105 (1999) 780–787.

[22] G. Gutiérrez-Urueta, P. Rodríguez, F. Ziegler, A. Lecuona, M.C. Rodríguez-Hidalgo, Extension of the characteristic equation to absorption chillers with adiabatic absorbers, Int. J. Refrig. 35 (2012) 709–718. https://doi.org/10.1016/j.ijrefrig.2011.10.010.

[23] M. Puig-Arnavat, J. López-Villada, J.C. Bruno, A. Coronas, Analysis and parameter identification for characteristic equations of single- and double-effect absorption chillers by means of multivariable regression, Int. J. Refrig. 33 (2010) 70–78. https://doi.org/10.1016/j.ijrefrig.2009.08.005.

[24] H. Hellmann, C. Schweigler, F. Ziegler, A simple method for modeling the operating characteristics of absorption chillers, in: Thermodyn. Heat Mass Transf. Refrig. Mach. Heat Pumps Semin. EUROTHERM 59, France, 1998: pp. 219–226.

[25] J. Albers, A. Kühn, S. Petersen, F. Ziegler, Control of absorption chillers by insight: the

characteristic equation, Czas. Tech. Mech. 105 (2008) 3–12. https://repozytorium.biblos.pk.edu.pl/resources/33958.

[26] J. Albers, F. Ziegler, Influence of internal irreversibilities on the characteristic equation of absorption chillers, in: Heat Powered Cycles Conf. Sept. 7-9, Berlin, Germany, 2009: pp. 69–70.

[27] J. Albers, Extension of a calculation method for the regulation of absorption refrigeration systems (in German), PhD TU Berlin, 2019.

[28] F. Boudéhenn, H. Demasles, J. Wyttenbach, X. Jobard, D. Chèze, P. Papillon, Development of a 5 kW cooling capacity ammonia-water absorption chiller for solar cooling applications, Energy Procedia. 30 (2012) 35–43. https://doi.org/10.1016/j.egypro.2012.11.006.

[29] D. Salavera, A. Coronas, Property Modeling of the Ammonia + Lithium Nitrate Mixture from New Experimental Data for Absorption Refrigeration Applications, in: 6th Int. Conf. Cryog. Refrig. April 12-14, Shanghai, China, 2018.

[30] R.L. Rowley, W.V. Wilding, J.L. Oscarson, N.F. Giles, DIPPR Data Compilation of Pure Chemical Properties, in: Design Institute for Physical Properties, New York, 2010.

[31] A. Altamirano, B. Stutz, N. Le Pierrès, A. Coronas, Experimental characterization by thermal and mass effectivenesses of plate heat exchangers in NH3-LiNO3 absorption chillers, in: ISHPC 2021 – Online Pre-Conference, Berlin, Germany, 2020: pp. 56–60. https://doi.org/10.14279/depositonce-10430.2.

[32] B. Michel, N. Le Pierrès, B. Stutz, Performances of grooved plates falling film absorber, Energy. 138 (2017) 103–117. https://doi.org/10.1016/j.energy.2017.07.026.

[33] C.M. Rops, R. Lindken, J.F.M. Velthuis, J. Westerweel, Enhanced heat transfer in confined pool boiling, Int. J. Heat Fluid Flow. 30 (2009) 751–760. https://doi.org/10.1016/j.ijheatfluidflow.2009.03.007.

[34] T.L. Bergman, A.S. Lavine, F.P. Incropera, D.P. Dewitt, Fundamentals of Heat and Mass Transfer, 7th editio, John Wiley & Sons, Inc., 2011.

[35] C. Amaris Castilla, Intensification of NH_3 Bubble Absorption Process using Advanced Surfaces and Carbon Nanotubes for NH_3/$LiNO_3$ Absorption Chillers, PhD Universitat Rovira i Virgili, 2013.

[36] A. Zacarías Santiago, Heat and mass transfer in adiabatic absorbers with the use of the lithium nitrate-ammonia solution (in Spanish), PhD Universidad Carlos III de Madrid, 2009.

[37] M. Mittermaier, F. Ziegler, Theoretical evaluation of absorption and desorption processes under typical conditions for chillers and heat transformers, Int. J. Refrig. 59 (2015) 91–101. https://doi.org/10.1016/j.ijrefrig.2015.07.015.

[38] M. Zamora, M. Bourouis, A. Coronas, M. Vallès, Pre-industrial development and experimental characterization of new air-cooled and water-cooled ammonia/lithium nitrate absorption chillers, Int. J. Refrig. 45 (2014) 189–197. https://doi.org/10.1016/j.ijrefrig.2014.06.005.

[39] M. Venegas, A. Zacarías, C. Vereda, A. Lecuona, R. Ventas, Subcooled and saturated boiling of ammonia-lithium nitrate solution in a plate-type generator for absorption machines, Int. J. Heat Mass Transf. 55 (2012) 4914–4922. https://doi.org/10.1016/j.ijheatmasstransfer.2012.04.061.

[40] V.P. Carey, Liquid-vapor phase-change phenomena, 1st ed., Taylor and Francis, 1992.